MINISTRY OF EDUCATION AND TRAINING

HO CHI MINH CITY UNIVERSITY
OF TECHNOLOGY AND ENGINEERING

NGUYEN LE DUY LUAN

IMPACT ASSESSMENT AND PENETRATION LEVEL DETERMINATION OF SOLAR PHOTOVOLTAIC SYSTEMS ON MEDIUM-VOLTAGE DISTRIBUTION NETWORKS

Major: Electrical Engineering (EE)
Major code: 9520201

SUMMARY OF DOCTORAL THESIS

HO CHI MINH CITY – 2026

This dissertation was completed at the **Ho Chi Minh City University of Technology and Engineering**

Thesis supervisor 1: Assoc. Prof. Dr. Vo Viet Cuong
Thesis supervisor 2: Assoc. Prof. Dr. Vo Ngoc Dieu

Reviewer 1:
Reviewer 2:
Reviewer 3:

The dissertation will be defended on .... before the Institutional Dissertation Evaluation Committee convened at Ho Chi Minh City University of Technology and Engineering.

LIST OF PUBLICATIONS

International articles

1. Le Duy Luan Nguyen, Phuc Khai Nguyen, Viet Cuong Vo, Ngoc Dieu Vo, Thang Trung Nguyen, and Tan Minh Phan, "Applications of Recent Metaheuristic Algorithms for Loss Reduction in Distribution Power Systems considering Maximum Penetration of Photovoltaic Units," International Transactions on Electrical Energy Systems, vol.23, article ID 9709608, 2003.

Domestic articles

1. Nguyen Phuc Khai, Nguyen Le Duy Luan, Pham An Thai, Vo Ngoc Dieu, Vo Viet Cuong, Phan Thanh Vinh, "A Methodology for Optimizing Curtailment of Solar Rooftops for Distribution Grids in Binh Thuan Province," The University of Danang Journal of Science and Technology, vol.21, no.10, pp. 85-89.

International conference

1. Luan D. L. Nguyen, Nguyen Hoang Phuong, Luc G. Le, Long N. T. Tran, Dieu, N. Vo, Cuong V. Vo, "Active power losses and the maximum penetration of PV in the MV distribution grid: Case-study of Pleiku, Vietnam," In Proceedings of the 2023 International Conference on System Science and Engineering (ICSSE), pp. 337-342, IEEE, Ho Chi Minh City, July, 2023.

Other scientific works related to the dissertation

1. Ministrial-level science and technology project "Research on Determining the Maximum Permissible Penetration Level of Renewable Energy Sources into Medium-Votage Grids," under the program "Research on Proposing Solutions to Enhance the Utilization Efficiency of Solar and Wind Power when Connected to the National Power Systems in the Central Region." Host institution: The University of Danang; code CT2022.07-DNA-09; Ministry of Education and Training; accepted in September 2025.
2. Ngoc Thien Le, Tran Hong An, Nguyen Le Duy Luan, Truong Cong Dinh, Le Thuong Du, Nguyen Van Son, Nguyen Hoang Minh Vu, Dinh Ngoc Sang, "Exploring the potentials applications of community solar system for greenfield project in Vietnam," In Proceedings of the 1st International Symposium on Power, Energy and Cybernetics (ISPEC), Hanoi, 18-19 Dec, 2020.

CHAPTER 1. INTRODUCTION

1.1. Statement of the problem

Rooftop photovoltaic (RPV) is central to the grid's distributed generation (DG) structure. Utility-scale PV connects centrally at the transmission level, whereas RPV sits behind the meter, dispersed across the distribution level. Its natural distribution, weather dependence, and reliance on customers' voluntary investment make RPV a highly unpredictable form of DG: at high penetration, peak RPV output can exceed local load and drive reverse power flow. The medium-voltage (MV) grid then faces (1) voltage violations; (2) lines and transformers overloading; (3) degraded power quality; and (4) protective relay miscoordination. Of these, voltage violations are widely reported as the key constraint limiting the RPV penetration level into the MV grid. To maximize RPV penetration, a careful assessment of penetration effectiveness to mitigate adverse impacts is essential.

1.2. Research gaps

For decades, research on RPV integration into MV grids has focused only on static-state optimization under discrete scenarios; few studies capture the variable nature of RPV or real-time uncertainties. This remains an open research gap. Recently, deep reinforcement learning (DRL) has emerged as a means to solve real-time, multi-objective grid-control problems.

Hosting capacity (HC) is the ratio of maximum installed DG capacity to peak load demand; available hosting capacity (AHC) denotes the maximum DG capacity accommodated at a given node or grid zone at a specific instant, reflecting the true penetration capability of DG once grid operational control schemes are integrated.

1.3. Objectives and research directions

The dissertation evaluates high RPV penetration impacts on MV grid voltage, current, and power losses to determine and maximize hosting capacity (HC). The research objectives are realized through four sequential phases: (1) quantifying grid impacts under high RPV penetration; (2) formulating a stochastic RPV curtailment model to mitigate adverse grid effects; (3) developing an optimization algorithm to determine maximum HC; and (4) proposing a hybrid DRL and artificial neural network (ANN) model for operational grid control to enhance penetration levels.

1.4. Research objects

- RPV systems with an installed capacity below 1 MW (equivalent to 1.25 MW_p);
- A radial 22 kV MV grid, or part thereof, with integrated RPV;
- The standard IEEE 33-bus and 69-bus test networks;
- On-load tap changers (OLTC) and smart inverters (SI);
- Stochastic metaheuristic (MH) optimization algorithms – the Coot optimization algorithm (COOA) and the Bat algorithm (BA);
- The hybrid DRL-ANN model.

1.5. Research scopes

- RPV capac with an installed capacity below 1 MW (equivalent to 1.25 MW_p);

- The standard IEEE 33-bus and 69-bus test networks, with real-world validation on a reference 22 kV MV feeder in Central Vietnam;
- Power losses, voltage fluctuations, and operating currents in the grid;
- Exclusions: transient or fault conditions; concurrent impacts from other RE sources, electric vehicles, BESS, or control devices excluding OLTC and SI.
- Regulatory framework: current Vietnamese RPV development policies.

1.6. Research methods

The dissertation adopts a multifaceted methodological approach, encompassing systematic literature review and analytical synthesis, computational modeling and simulation, empirical field investigations as well as scenario-based forecasting.

1.7. Practical contributions of the dissertation

- Alignment with National context: The research trajectory mirrors the Vietnam's PV evolution. This progression transitions from an initial phase of exponential, loosely regulated expansion – driven by the FIT-1 and FIT-2 incentive mechanisms – through a consolidation phase necessitating in-depth investigation, to the current paradigm of controlled development facilitated by integrated grid management. The findings obtained at each phase therefore provide a valuable reference for addressing pressing challenges in operational practice.
- Rigorous validation: Proposed models are validated on standard IEEE test feeders and demonstrate high viability for real-world grid deployment;
- Data-driven resilience: The DRL model effectively mitigates typical MV grid constraints, such as sparse historical operational data, fragmented remote metering, and limited SCADA infrastructure;
- Regulatory and utility frameworks: The dissertation provides utilitites with a technical framework for RPV interconnection appraisals and offer regulators a scientific foundation to update national MV grid integration regulations;
- Academic value: The simulated datasets and models serve as educational resources and benchmarks for future RE integration research.

1.8. Dissertation structure

Chapter 1. Introduction

Chapter 2. Theoretical background

Chapter 3. Determining the maximum penetration level and optimal RPV curtailment: Application in Vietnam

Chapter 4. Metaheuristic optimization for determining the maximum RPV penetration level

Chapter 5. Applying a DRL model to enhance RPV penetration capability in MV grids

Chapter 6. Conclusion and future works

CHAPTER 2. THEORETICAL BACKGROUND

2.1. Overview of RPV impacts on the MV grid

The number of literature examining impacts on MV grids expanded significantly during 2015 – 2019, reflecting accelerating global penetration. [1] categorizes four intrinsic attributes of RPV, namely its distributed topology, diurnal generation profile, inverter-based interfacing, and stochastic intermittency, which drive four primary grid impacts: voltage volatility, power losses induced by reverse power flow, protection miscoordination, and power quality degradation. Among these, voltage issues, comprising unbalance, fluctuations, and overvoltage at the point of common coupling (PCC), remain the critical technical constraints limiting grid HC.

2.2. Tools for assessing RPV impacts on the MV grid

Empirical validation via direct field measurements provides maximum fidelity. Accelerated by advancements in computing, mathematical optimization, and AI, several key software and hardware-in-the-loop platforms are widely adopted to assess RPV impacts on MV grids: GAMS, MATLAB/Simulink, PLEXOS, MATPOWER, FESTIV, DIgSILENT, OpenDSS, PowerFactory, PSS/E, ETAP, RTDs, eMEGAsim, HYPERSIM, Typhoon HIL.

2.3. Models for assessing RPV impacts on the MV grid

Four distinct groups: (1) Deterministic models: Fix all input variables, offering the fastest computation and simplest implementation; (2) Probabilistic models: Characterize uncertain inputs via probability density functions, suitable for small-scale grids; (3) Quasi-static time-series models: The predominant approach in HC research, simulate large-scale networks across continuous temporal horizons with high fidelity; and (4) Data-driven operational models: Utilize smart-metering and SCADA infrastructure for high accuracy.

2.4. Power flow analysis

Power flow analysis applies the two Kirchhoff laws to a nonlinear circuit with varying voltage magnitudes and phase angles. The complex power equation is:

$$P_i - jQ_i = [|V_i|\angle(-\delta)].\sum_{j=1}^{n}|Y_{ij}||V_j|\angle\theta_{ij} + \delta_j \tag{2.1}$$

For power flow analysis, the Gauss-Seidel (GS) and Newton-Raphson (NR) methods are standard. The NR linearizes nonlinear algebraic equations, providing robust performance and quadratic convergence.

2.5. RPV power calculation

The RPV power injected into the grid is computed using a Gaussian model:

$$GHI(t) = GHI_{\text{max}} \times e^{\left[-\frac{1}{2}\left(\frac{t-t_{\text{noon}}}{\sigma_{\text{mt}}}\right)^2\right]}, t \in \left[t_{\text{mọc}}; t_{\text{lặn}}\right] \tag{2.2}$$

$GHI(t)$: the solar irradiance at hour t of the day, [$\mathrm{W/m^2}$]; GHI_{max}: the max irradiance at the peak hour t_{noon}, [$\mathrm{W/m^2}$]; σ_{mt} is the width of the Gaussian curve.

The capacity factor (CF) converts $GHI(t)$ into electrical power:

$$CF(t) = \frac{GHI(t)}{GHI_{\text{STC}}} \tag{2.3}$$

The RPV output of each node and for the entire grid is calculated as:

$$P_{\text{RPV},m}(t) = P_{\text{RPV},m}^{\text{đặt}} \times CF(t) \times \eta_1 \times \eta_2 \times \eta_3 \tag{2.2}$$

$$P_{\text{RPV,total}}(t) = \sum_{m \in \mathbb{R}} P_{\text{RPV},m}(t) \tag{2.3}$$

$\mathbb{R}$ is the set of nodes at which RPV is installed; $P_{\text{RPV},m}^{\text{đặt}}$ is the installed RPV capacity at node $m \in \mathbb{R}$, [kW]; η_1 is the derating factor due to the operating temperature of the solar cell; η_2 is the inverter efficiency và η_3 is the system loss.

2.6. Grid operating parameters calculation

2.6.1. Voltage fluctuation on the grid

The voltage drop on the grid, before and after RPV integration, is calculated as:

$$\Delta V_{\text{bf}} = \frac{P_{\text{load}}.R + jQ_{\text{load}}.X}{V_n} \tag{2.6}$$

$$\Delta V_{\text{af}} = \frac{[P_{\text{load}} - (\pm P_{\text{RPV}})].R + j[Q_{\text{load}} - (\pm Q_{\text{RPV}})].X}{V_n} \tag{2.7}$$

The voltage rise after integrating RPV into the grid is given by:

$$\Delta V_{\text{tăng}} = \frac{\Delta V_{\text{af}}}{V_{\text{ph\_n}}} \approx \frac{R_{\text{rp}}.P_{\text{o.RPV}}}{3V_n^2} \tag{2.8}$$

R and jX are the series resistance and reactance of the line, [Ω]; P_{load}, Q_{load} are the active [W] and reactive power [VAr] of the load; P_{RPV} and Q_{RPV} are the active and reactive power injected by the RPV system at the node; V_n is the rated system voltage, [V]; R_{rp} is the resistive component of the short-circuit impedance at PCC.

2.6.2. Power losses on the grid

The power loss differential explicitly quantifies the loss-abatement efficacy yielded by varying degrees of RPV penetration:

$$\Delta P = \sum_{k=1}^{N_{\text{br}}} \int_0^{\text{T}} P_{\text{RPV}}^t(t).\left[P_{\text{RPV}}^t(t) - 2P_{\text{load}.i}^t(t)\right].\mathrm{d}t \tag{2.9}$$

Where N_{br} is the number of feeders on the grid; T is the time interval considered, and $P_{\text{load}.i}(t)$ is the power consumed on branch k at hour t, [kW].

If $\Delta P > 0$, the losses increase. Conversely, if $P_{\text{RPV}}^t(t) - 2P_{\text{tải}.i}^t(t) < 0$ then $\Delta P < 0$, meaning that the system losses decrease.

2.6.3. Overload limits of lines and transformers and the maximum RPV output

After RPV integration, the load apparent power reaches its maximum when:

$$S_{\text{max.af}} = \sqrt{(P_{\text{RPV.max}} - P_{\text{load.min}})^2 + Q_{\text{load.min}}^2} \tag{2.10}$$

The maximum allowable active power injection from RPV systems:

$$P_{\text{RPV.max}} < P_{\text{load.min}} + \sqrt{S_{\text{max.bf}}^2 - Q_{\text{load.min}}^2} \tag{2.11}$$

2.7. Optimization and metaheuristics

2.7.1. Optimization in power systems

Optimization identifies the best solutions within a feasible region. Structurally, a model comprises three interconnected elements: an objective function to be extremized, a decision variable vector, and a constraint set. Optimization theory encompasses two paradigms: (1) deterministic analytical methods; (2) numerical approximation frameworks: rule-based heuristics, stochastic metaheuristics (MH), and self-adaptive hyperheuristics. Recently, AI-driven and hybrid approaches have emerged as prominent research and application trends.

2.7.2. Metaheuristic optimization and the maximum RPV penetration problem

MH maximize RPV penetration by stochastically balancing exploration and exploitation. Their generalized execution framework encompasses: (1) population initialization; (2) sub-population partitioning; (3) attribute evaluation against stochastic criteria; mathematical modeling of (4) exploration, (5) exploitation, and (6) stochastic selection/updating mechanisms, and (7) convergence validation.

2.8. RPV penetration into the MV grid

2.8.1. Definitions

HC defines the maximum DG capacity interconnectable without violating operational thresholds or necessitating infrastructure upgrades. Specifically, maximum RPV penetration (HC_{RPV}) denotes the upper bound of integrated RPV generation that strictly satisfies voltage, current, and power loss constraints.

$$HC_{\text{RPV}}(\%) = \frac{\sum_{m=1}^{n} P_{\text{RPV},m}}{P_{\max}}.100 \tag{2.12}$$

$P_{\text{RPV},m}$ is the installed capacity of the m^{th} RPV; $P_{\max}$ is the peak demand, [kW].

Available hosting capacity (AHC) denotes the maximum instantaneous RPV capacity permissible at a specific bus or zone subject to operational constraints, thereby quantifying the true integration capability enabled by grid control strategies

2.8.2. The maximum RPV penetration problem

The objective function for maximizing RPV penetration is:

$$F = \max_{P_{\text{RPV}}} \sum_{m \in \mathbb{R}} P_{\text{RPV},m} \tag{2.13}$$

HC_{RPV} is constrained by equipment thermal ratings, short-circuit withstand capacities, the $P_{\max}/P_{\text{RPV}}$ ratio; with thermal and fault tolerances taking priority. HC_{RPV} evaluation spanning 05 paradigms: deterministic, stochastic, scenario-based optimization, time-series, and network reduction. Incorporating operational control transitions the formulation to AHC, predicated on voltage margin and sensitivity analyses at integration nodes. Specifically, voltage sensitivity quantifies voltage fluctuations per incremental RPV injection to identifying critical nodes for control strategies, while voltage margin analysis establishes the remaining operational headroom exploitable for increased penetration [2].

2.8.3. Measures for enhancing RPV penetration in the MV grid

Enhancing MV grid RPV penetration is a multi-objective optimization problem addressed by 04 key measures: SI reactive power control, BESS integration, network reconfiguration, and OLTC-based voltage regulation. These measures yield reported improvement ranges of 45%-78%, 50%-111%, 50%-150%, and 50%-100%, respectively. In Vietnam, network configuration and OLTC regulation are already effectively deployed to mitigate high penetration challenges.

2.9. Deep reinforcement learning and its application in MV grids

DRL integrates the operational control efficacy of reinforcement learning with the advanced telemetry processing and forecasting capabilities of deep learning (DL), providing a continuous updating mechanism to solve nonlinear issues.

Formulated as a Markov Decision Process (MDP) defined by the 5-tuple $\{S, A, \Psi, R, \gamma\}$, an agent at step t maps state $s_t \in S$ to action $a_t \in A$, receiving reward r_t and transitioning to s_{t+1} to maximize the expected cumulative reward under an optimal policy π_{optimal}. Consequently. DRL effectively resolves HC_{RPV} and AHC problems through model-free, real-time autonomous adaptation within high-dimensional, nonlinear, and uncertain grid environments.

CHAPTER 3. DETERMINING THE MAXIMUM PENETRATION LEVEL AND OPTIMAL RPV CURTAILMENT: APPLICATION IN VIETNAM

3.1. Statement of the problem

Driven by high irradiance, Vietnam's PV capacity is projected to exceed 30% of the generation mix by 2050 [3]. However, severe geographic generation imbalances cause reverse power flows exceeding 59% (South) and 33.78% (Central), overloading MV feeders during peak-irradiance, low-demand periods and forcing generation curtailment.

3.2. Determining the maximum RPV penetration level in the MV grid by the deterministic method

This study evaluates RPV integration impacts on MV network power losses and deterministically quantifies maximum penetration level under static operational constraints. The assessment utilizes a time-domain unbalanced load-flow (TDULF) framework applied to feeder 472 C42/DHO of the Pleiku grid, Gia Lai province.

3.2.1. Flowchart

3.2.2. Input data

Input data encompass cable specifications, transformer parameters, historical load profiles (P, Q, V, I), and PVGIS-derived solar irradiance time-series.

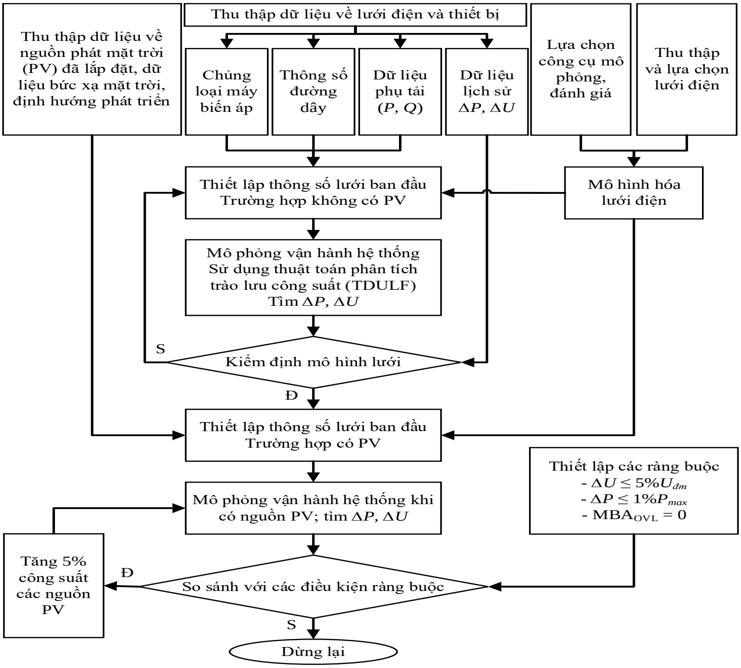

Fig 3.1. Flowchart for determining the maximum penetration level of RPV to MV grid by deterministic method

3.2.3. Results and discussion

Pleiku's distinct biseasonal climate drives highly variable, predominantly residential demand fluctuating across seasonal, weekly, and hourly scales. Four representative days are selected to examine the impact of RPV on grid losses: a dry-season weekday (DSW), a dry-season weekend (DSE), a rainy-season weekday (RSW), and a rainy-season weekend (RSE).

During DSW and DSE scenarios, RPV integration mitigates network losses, shifting the baseline peak from 19:30 to 17:30 – 19:00 and reducing peak-irradiance losses from 0.78% to 0.52%. Conversely, cloud-induced intermittency during RSW and RSE profiles causes volatile fluctuations with negligible impact average or maximum (~0.58%) losses, confirming season-dependent mitigation efficacy.

Worst-case simulation reveal critical boundaries: bus overvoltage initiates at an 85% penetration threshold, while transformers overloading occurs past 135% of peak load. This demonstrates a parabolic loss trajectory: initial penetration offsets local demand but excessive integration reverses power flows, inducing overcurrent and escalating network losses.

Ultimately, these empirical findings validate model soundness, proving the deterministic analytical method is a computationally efficient framework for rapid estimation of RPV penetration to strategically optimize grid loss profiles.

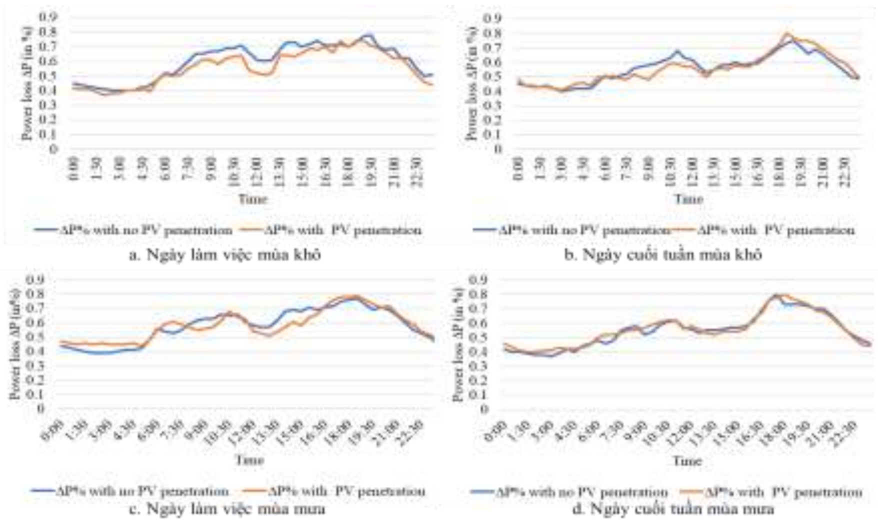

Fig 3.2. Simulation results for active power losses

3.3. Bat algorithm model for optimal RPV power curtailment

RPV power curtailment has occurred in the US, Germany, China, and Chile due to infrastructure constraints under rapid, large-scale penetration. Similarly, Vietnam must curtail PV output during peak-irradiance, low-demand periods. However, the theoretical basis for optimal curtailment has not yet been thoroughly examined or computed in detailed studies for Vietnam.

3.3.1. Introduction to the Bat algorithm

The BA is applied to DG planning, dispatch, voltage control, RPV curtailment, and grid congestion management [4] using three approximating conditions: (1) all bats use echolocation to sense distance and to distinguish prey from obstacles; (2) each bat flies at velocity v_i at position x_i, with a fixed frequency $f_{\min}$, wavelength λ, and loudness A_0 to search for prey; and (3) the loudness remains positive, varies strictly within the range $[A_0; A_{\min}]$. Throughout the optimization process, the frequency f, position x_i, and velocity v_i are continuously updated.

3.3.2. Objective function formulation

The optimization objective minimizes cumulative RPV generation curtailment

$$F(x) = \sum_{t=7}^{17} \sum_{1}^{N_{\mathrm{RPV}}} P_{m,t}^{\mathrm{cur}} = \sum_{t=7}^{17} \sum_{1}^{N_{\mathrm{RPV}}} \left(P_{\mathrm{RPV},m,t}^{\max} - P_{\mathrm{RPV},m,t}^{\mathrm{pen}}\right) \tag{3.1}$$

$P_{m,t}^{\mathrm{cur}}$, $P_{\mathrm{RPV},m,t}^{\max}$, and $P_{\mathrm{RPV},m,t}^{\mathrm{pen}}$ are the curtailment power, the maximum output power, and the allowable output power at the m^{th} RPV bus at hour t, [kW].

3.3.3. Constraints

– RPV output power:

$$0 \le P_{\mathrm{RPV},m,t} \le P_{\mathrm{RPV},m,t}^{\max} \tag{3.2}$$

– Line current constraint: Branch operating currents $\left(I_{op,k}\right)$ are bounded by cable ampacity (I_k^{max}).

$$I_k^{\max} \geq I_{op,k} \text{ với } k = 1, 2, \dots, N_{\text{br}} \tag{3.3}$$

– Bus voltage limit:

$$V_{\min} \leq V_{\text{nút},i} \leq V_{\max} \text{ với } i = 1, 2, \dots, \mathrm{N}_{\text{nút}} \tag{3.4}$$

– Power balance equation:

$$P_0 + \sum_{m=1}^{N_{\text{RPV}}} P_{\text{RPV},m} - \sum_{i=1}^{N_{\text{nút}}} P_{\text{load},i} - \sum_{k=1}^{N_{\text{br}}} P_{\text{loss},k} = 0 \tag{3.5}$$

$$Q_0 + \sum_{m=1}^{N_{\text{RPV}}} Q_{\text{inv},m} - \sum_{i=1}^{N_{\text{nút}}} Q_{\text{load},i} - \sum_{k=1}^{N_{\text{br}}} Q_{\text{loss},k} = 0 \tag{3.6}$$

3.3.4. BA application to the 471LS Binh Thuan feeder curtailment problem

The 471LS feeder contains 582 MV buses, 316 segments, 196 substations, two 0.3-MVAr capacitors, and ten RPV sources (9.28 MWp total). Temporal mismatches between peak RPV generation at 11:00 and peak demand at 17:00 drive reverse power flows and feeder overloading.

To optimize curtailment, the BA defines candidate solutions as vector $x_i = x_{\text{cur}}$ in the search space for $d = N_{\text{RPV}}.n_t$ daily time-steps, penalizing constraint violations via objective function augmentation.

$$\tilde{F}(x) = F(x) + \omega_V.\sum_{i=1}^{N_{\text{nút}}} \max\left(V_i - V_{\max}, 0\right) + \omega_S \sum_{j=1}^{N_{\text{br}}} \max\left(S_{ij} - S_{ij}^{\max}, 0\right) \tag{3.7}$$

Where V_i is the voltage at bus i, [p.u.]; S_{ij} is the power flow on branch ij, [MVA]; ω_V, ω_S are the penalty coefficients for constraint violations, typically chosen within the range $[10^3; 10^4]$.

The BA configuration employs a population of 20 over 200 iterations, with a frequency range of $[0; 2]$, initial loudness of 1.0, and initial emission rate of 0.5; both adaptation coefficients are set to 0.9.

Fig. 3.3 delineates the optimization flowchart.

3.3.5. Results and discussion

– RPV curtailment when the source voltage is below 1,010 p.u.

Three weather-driven RPV generation scenarios are evaluated: sunny (100%), cloudy (40%), and rainy (10%), with diurnal load-generation profiles (07:00 to 17:00) illustrated in Fig. 3.4. At 12:00, peak outputs of 1.217 MW (rainy) and 4.043 MW (cloudy) induce no operational violations, rendering curtailment unnecessary. Conversely, maximum sunny-day generation triggers feeder overloading and over-voltage, necessitating curtailment. Furthermore, given source voltage (V_0) impacts on grid-wide profiles, sensitivity is analyzed across seven discrete levels from 1.000 to 1.030 p.u. in 0.005 p.u. increments.

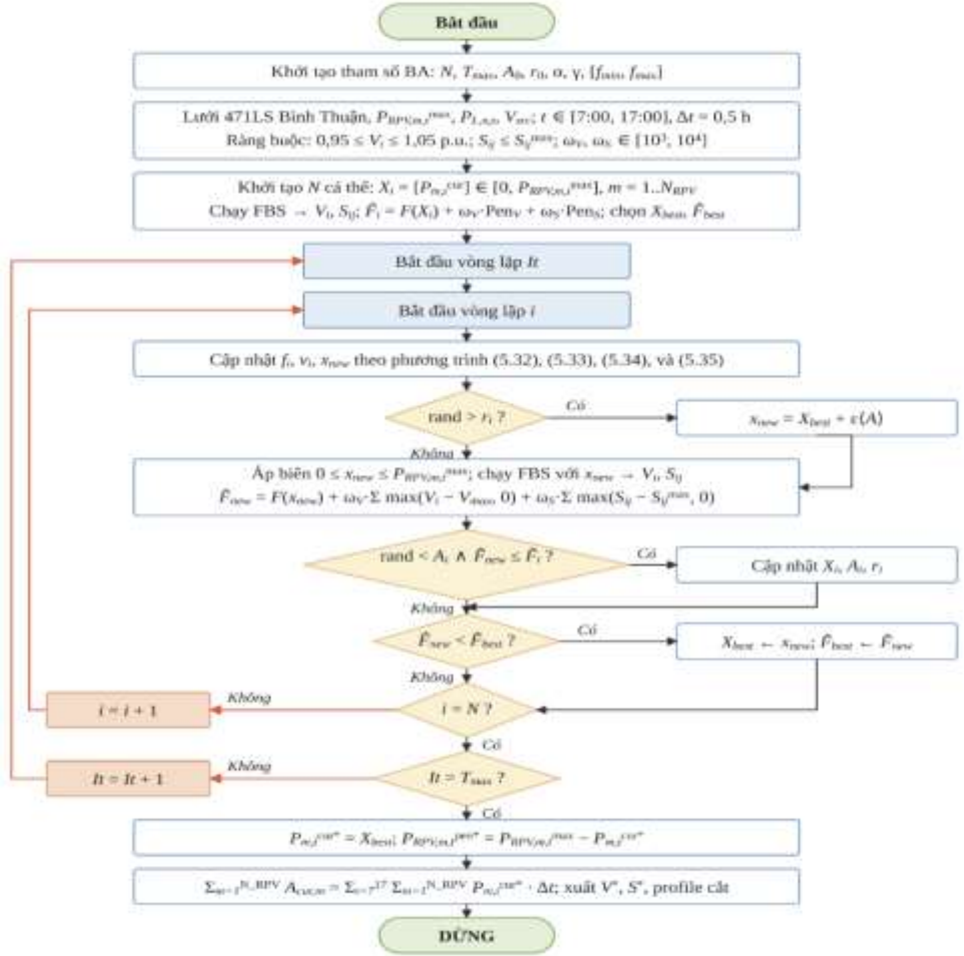

Fig. 3.3. Flowchart for determining the optimal RPV curtailment power by BA

Across all weather and source-voltage configurations, RPV integration induces no overvoltage. Sunny-day generation exceeds demand by 308%, necessitating either reverse-flow allowance or equitable grid-wide curtailment. Maintaining V_0 below 1.010 p.u. exploits feeder generation capacity, maximizing RPV penetration at 190.4% under strict power-quality compliance.

– RPV curtailment when the source voltage ranges from 1,010 to 1,030 p.u.

Cloudy and rainy scenarios yield zero violations. Conversely, sunny-day peak irradiance (12:00) triggers severe voltage stress: V_0 scaling at 1.010, 1.015, 1.020, 1.025, and 1.030 p.u. induces 25, 176, 353, 466, and 353 violating buses, requiring BA-driven targeted curtailments of 2.80, 19.32, 23.61, 25.79, and 30.27 MWh, respectively, to restore complete grid compliance.

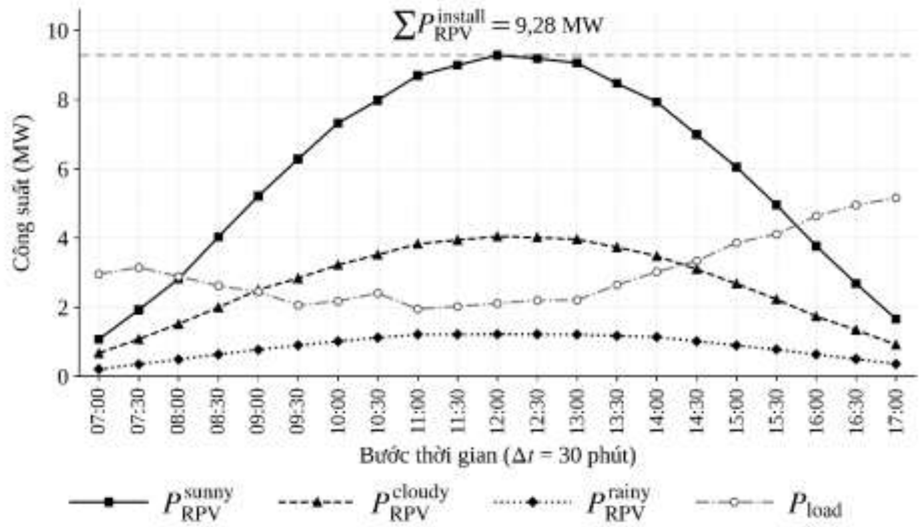

Fig 3.4. Diurnal load-generation profile

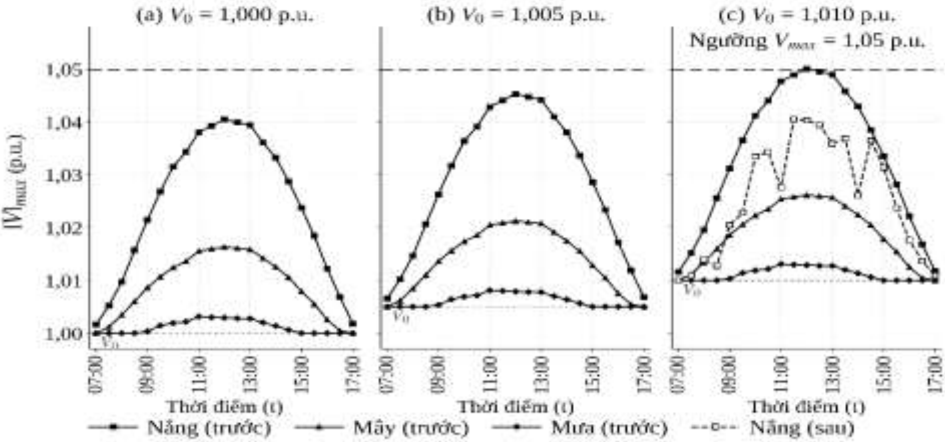

Fig 3.5. Hourly voltage profiles across varying weather scenarios and source-voltage levels

These results demonstrate that the BA maximally exploits operational constraint margins. The non-uniform allocation across RPV assets underscores a sensitivity-driven optimization strategy that preferentially curtails sources proximate to peak-voltage nodes.

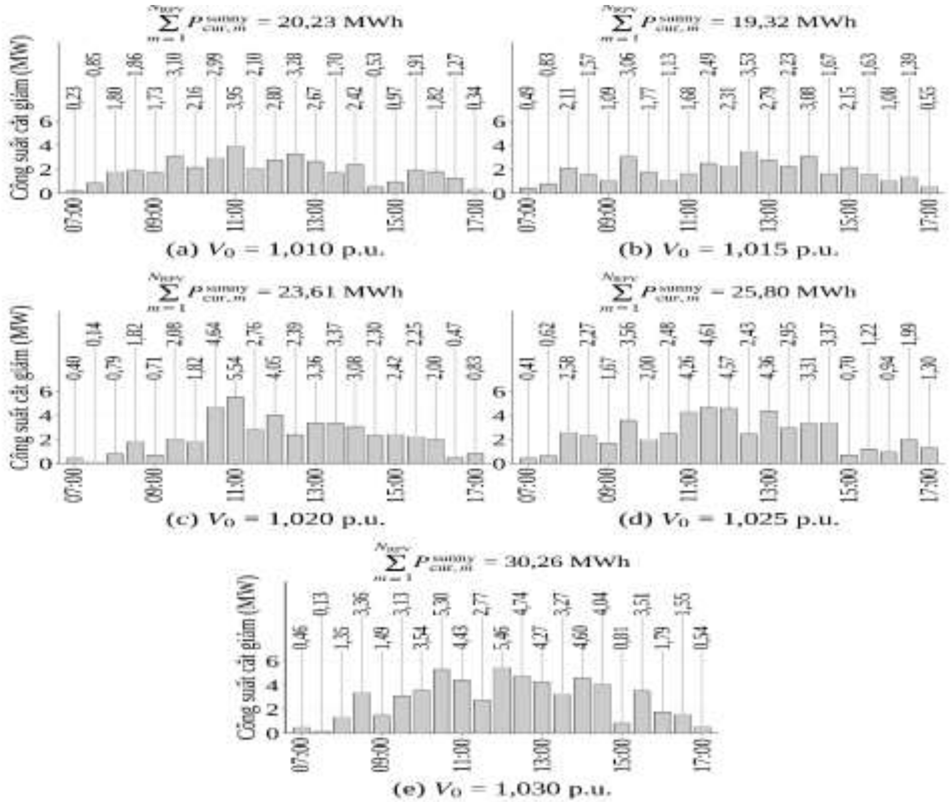

Fig 3.6. Hourly voltage profiles across three weather scenarios and four source-voltage levels

CHAPTER 4. METAHEURISTIC OPTIMIZATION FOR DETERMINING THE MAXIMUM RPV PENETRATION LEVEL

4.1. Statement of the problem

Line impedance governs active and reactive power losses (P_{loss} và Q_{loss}) alongside voltage fluctuations (ΔV), which scale directly with branch operating currents ($I_{op,k}$). Consequently, load escalations exacerbate these metrics, whereas RPV integration modulates net demand, dynamically shifting $I_{op,k}$, ΔP và ΔV.

4.2. COOA-based maximum RPV penetration level quantification

4.2.1. Objective function formulation

While conventional MH studies for MV-grid RPV integration predominantly prioritize loss minimization, this work formulates the maximum penetration objective function as:

$$\mathrm{F} = \min \sum_{k=1}^{N_{\mathrm{br}}} P_{\mathrm{loss},k} \tag{4.1}$$

$P_{\mathrm{loss},k}$ is the power loss of branch k, [kW]; N_{br} is the number of feeders.

4.2.2. Constraints

– Bus voltage boundaries: regulated per (3.4)

– RPV siting constraint: restricted to non-slack nodes

$$2 \le L_{\mathrm{RPV},p} \le N_{\text{nút}} \text{ với } p = 1, 2, \dots, N_{\text{nút}} \tag{4.2}$$

– Aggregate RPV capacity: bound by total penetration limits

$$\sum_{m=1}^{N_{\mathrm{RPV}}} P_{\mathrm{RPV},m}^{\text{đặt}} \le \sum_{i=1}^{N_{\text{nút}}} P_{\mathrm{load},i} + \sum_{k=1}^{N_{\mathrm{br}}} P_{\mathrm{loss},k} \tag{4.3}$$

– Line current thermal limit: enforced via formulation (3.3)

– RPV reactive power and power factor: confined to operational boundaries

$$PF^{\min} \le PF_{\mathrm{RPV},m} \le PF^{\max} \tag{4.4}$$

$$\sum_{m=1}^{N_{\mathrm{RPV}}} Q_{\mathrm{inv},m} \le \sum_{i=1}^{N_{\text{nút}}} Q_{\mathrm{load},i} \le \sum_{k=1}^{N_{\mathrm{br}}} Q_{\mathrm{loss},k} \tag{4.5}$$

– Power balance equilibrium: governed by formulations (3.5) and (3.6).

4.2.3. COOA application for maximizing MV-grid RPV penetration

The COOA optimizes RPV penetration through irregular and synchronized phases. Utilizing a distinct updating and selection mechanism, COOA guides optimization via four strategic movements: random, chain, group-leader tracking, and leader adaptation [5]. Fig. 4.1 traces the comprehensive optimization flowchart.

The initial population is randomly initialized via equation (4.6), with the leader-coot (LC) group capped at 20%

$$X_i = \mathrm{random}(1, D).\left(X^{\max} - X^{\min}\right) + X^{\min}; i = 1, \dots, \mathrm{No}_p \tag{4.6}$$

The optimization control variables comprise the capacity, power factor, and grid siting of each RPV, with each candidate solution vector X_i formulated as:

$$X_i = \left[P_{\mathrm{RPV},m,i}, PF_{\mathrm{RPV},m,i}, L_{\mathrm{RPV},m,i}\right]; m = 1, \dots, N_{\mathrm{RPV}} \tag{4.7}$$

A backward – forward sweep algorithm computes the dependent variables $(P_{ij}, Q_{ij}, V_j, I_{op,k})$, then they yield $P_{\mathrm{loss},k}$, ΔV_i và $\Delta I_{op,k}$. The fitness function is:

$$Fit_i = P_{\mathrm{loss},i} + \beta \sum_{k=1}^{N_{br}} \left(\Delta I_{op,k}\right)^2 + \beta \sum_{i=1}^{N_{\text{nút}}} (\Delta V_i)^2 \tag{4.8}$$

The 20% of solutions with the best fitness are placed in the LC group, and the iterative process continues until the best coot is found. At each output, the solution is updated as follows:

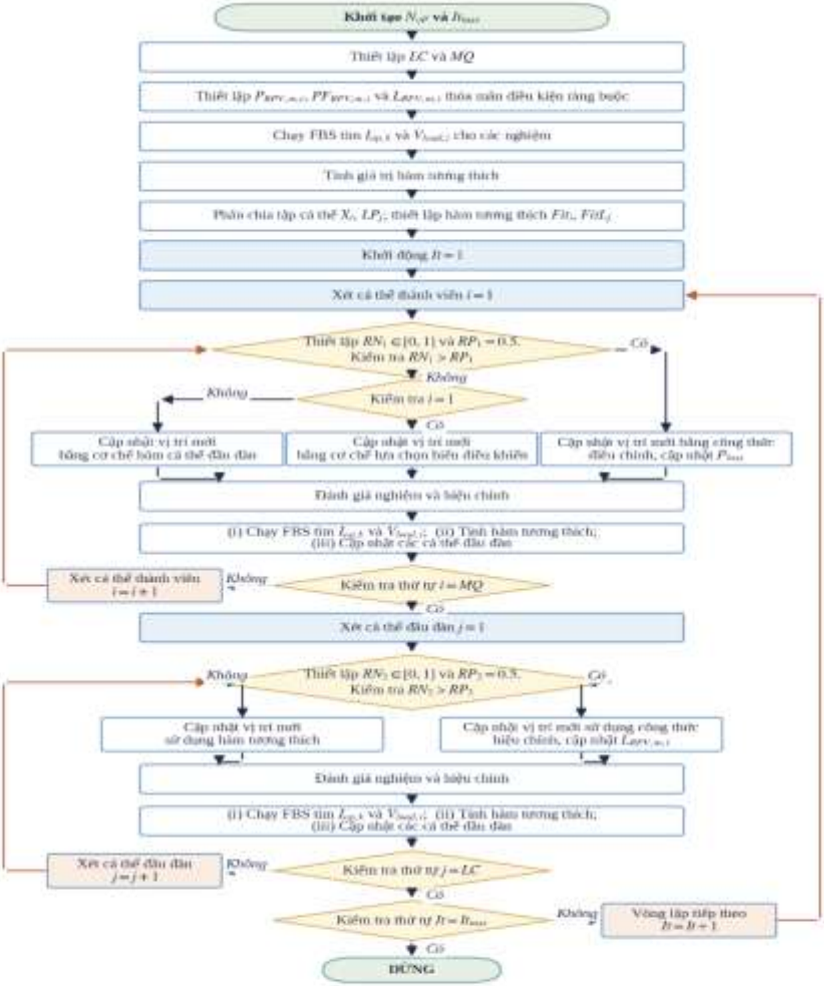

Fig 4.1. Flowchart of the proposed COOA-based maximum RPV penetration quantification

$$L_{\mathrm{RPV},m,i}^{\mathrm{new}} = \begin{cases} L_{\mathrm{RPV},m,i}^{\mathrm{new}} \text{ if } L_{\mathrm{RPV},m,i}^{\mathrm{new}} \in [2;\ N_{\text{nút}}] \\ N_{\text{nút}} \text{ if } N_{\text{nút}} < L_{\mathrm{RPV},m,i}^{\mathrm{new}} \\ 2 \text{ if } L_{\mathrm{RPV},m,i}^{\mathrm{new}} < 2 \end{cases} ;m = 2, \dots, N_{\text{nút}} \tag{4.9}$$

$$P_{\mathrm{RPV},m,i}^{\mathrm{new}} = \begin{cases} P_{\mathrm{RPV},m,i}^{\mathrm{new}} \text{ if } P_{\mathrm{RPV}}^{\min} \le P_{\mathrm{RPV},m,i}^{\mathrm{new}} \le P_{\mathrm{RPV}}^{\max} \\ P_{\mathrm{RPV}}^{\min} \text{ if } P_{\mathrm{RPV}}^{\min} > P_{\mathrm{RPV},m,i}^{\mathrm{new}} \\ P_{\mathrm{RPV}}^{\max} \text{ if } P_{\mathrm{RPV}}^{\max} < P_{\mathrm{RPV},m,i}^{\mathrm{new}} \end{cases} ;m = 1, \dots, N_{\mathrm{RPV}} \tag{4.10}$$

$$PF_{\mathrm{RPV},m,i}^{\mathrm{new}} = \begin{cases} PF_{\mathrm{RPV},m,i}^{\mathrm{new}} \text{ if } PF_{\mathrm{RPV}}^{\min} \le PF_{\mathrm{RPV},m,i}^{\mathrm{new}} \le PF_{\mathrm{RPV}}^{\max} \\ PF_{\mathrm{RPV}}^{\min} \text{ if } PF_{\mathrm{RPV}}^{\min} > PF_{\mathrm{RPV},m,i}^{\mathrm{new}} \\ PF_{\mathrm{RPV}}^{\max} \text{ if } PF_{\mathrm{RPV}}^{\max} < PF_{\mathrm{RPV},m,i}^{\mathrm{new}} \end{cases} \quad (4.11)$$

The leader coots use the best-position mechanism to update their positions.

The framework is validated on standard IEEE 33-bus [6] and 69-bus [7] networks across four simulation cases: (1) C_1S_1 and C_1S_2: Fix N_{RPV} and PF_{RPV}, find L_{RPV} and $P_{\mathrm{RPV}}^{\text{đặt}}$; (2) C_2S_1 and C_2S_2: Fix N_{RPV}, find 03 remain parameters; (3) C_3S_1 and C_3S_2: Fix PF_{RPV}, find 03 remain parameters; and (4) C_4S_1 and C_4S_2: Find all variables.

4.2.4. Results and discussion

– Simulation results on the 33-bus radial network

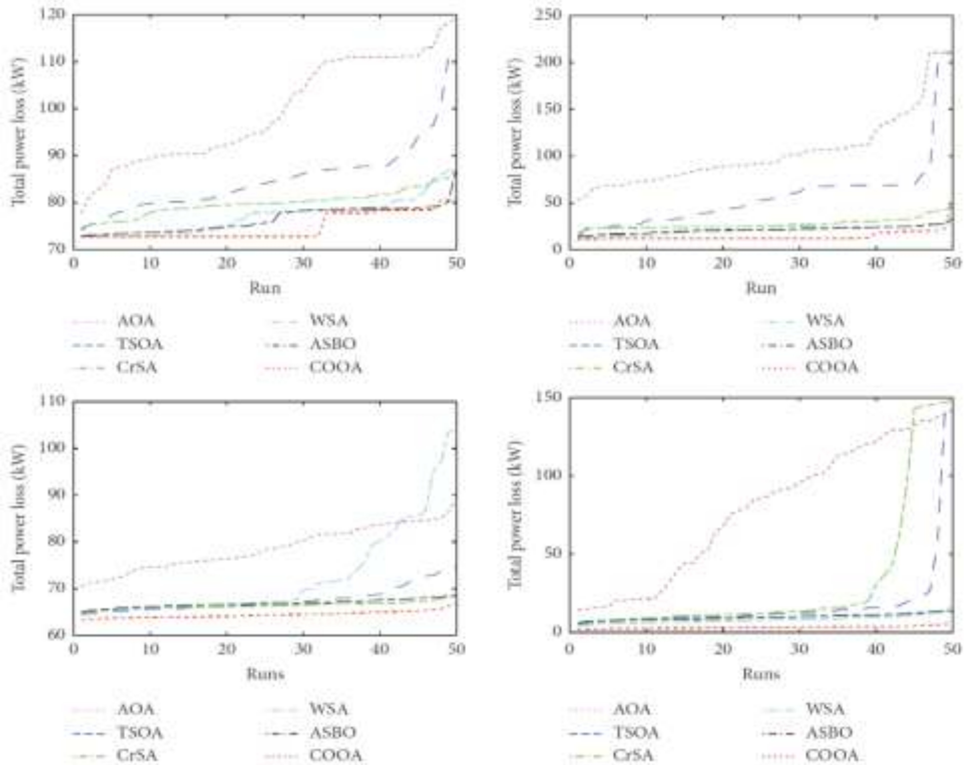

Fig 4.2. Comparison of simulation results across scenarios on the 33-bus grid

As validated in Fig. 4.2, COOA outperforms 23 benchmark MHs by ensuring minimal grid losses and absolute convergence stability (~zero variance over 30 independent runs) against severe run-to-run stochastic volatility. For scenarios C_1S_1 and C_2S_1, COOA secures loss reduction metrics of 65.5% and 94.4% alongside penetration levels of 75.1% and 89.3%, respectively, under a computational execution averaging 8.3 seconds. For multi-source allocations, C_3S_1 yields a 70% loss mitigation at 93.5% penetration, distributing nine RPV units across nodes 3, 7, 10, 16, 21, 24, 25, 30, 32 (a three-node topological shift from ISOSA). Under C_4S_1, residual losses plunge to 1.66 kW (99.2% reduction) at 103.7% penetration within 34 seconds, strategically clustering assets at buses 6, 8, 14, 18, 21, 24, 25, 30 and 32, thereby altering the ISOSA baseline by four locations. These empirical metrics confirm the optimization efficacy of the proposed framework.

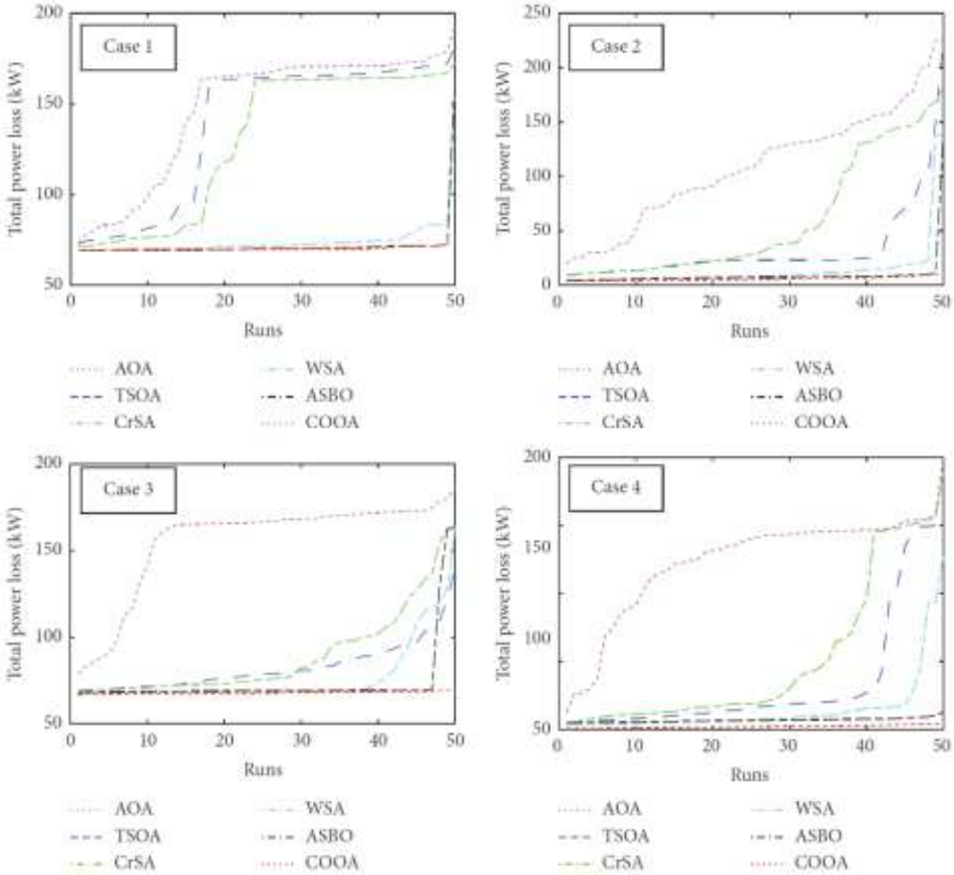

Fig 4.3. Comparison of simulation results across scenarios on the 69-bus grid

As illustrated in Fig. 4.3, COOA consistently outperforms benchmark MH across cases C_1S_2, C_2S_2, C_3S_2 and C_4S_2, securing minimal network losses and superior convergence stability with negligible run-to-run variance. Relative to the base case, COOA mitigates losses by 69.14% C_1S_2 and 98.10% C_2S_2, yielding peak load penetration levels of 65.2% and 77.5%, respectively, within a 10-20 seconds execution window. Conversely, under the highly constrained C_3S_2 and C_4S_2 configurations, $\%\Delta P_{\mathrm{re}}$ margins span 0.17% - 15.10% and 46.20 – 95.39% over 30-

40 seconds runs, achieving maximum penetration thresholds of 84.6% and 114.8%. To sustain these levels, COOA expands the topological allocation to nine strategic RPV sites: nodes 3, 8, 11, 15, 21, 33, 50, 61, 64 for C_3S_2 (versus the seven-site baseline of benchmark algorithms), and nodes 11, 12, 17, 22, 28, 49, 51, 61, 64 for C_4S_2. These empirical metrics validate the efficacy and reliability of COOA-driven static grid integration planning.

CHAPTER 5. APPLYING A DRL MODEL TO ENHANCE RPV PENETRATION CAPABILITY IN MV GRIDS

5.1. DRL framework for enhancing MV-grid RPV penetration

DRL dynamically adapts grid control policies via continuous state space observation and interactive learning. Its MV-grid applications encompass power system stability [8], peak-shaving/load-shifting optimization [9], voltage regulation [10], multi-source microgrid energy management [11], and security control [12]. DRL optimization features four core merits: model-free parameter independence, real-time adaptability to network volatility, reward-mapped operational constraints, and robust multi-objective resolution. Nevertheless, MV-grid DRL deployments remain critically underexplored in scope, volume, and rigorous empirical validation

5.2. Problem formulation for enhancing MV-grid RPV penetration

5.2.1. Multi-objective function formulation

– Maximization of HC_{RPV}:

$$F_1 = \max \sum_{t=0}^{23} \sum_{m \in \mathbb{R}} P_{RPV}(m,t,a) \tag{5.1}$$

– Minimization of active power losses:

$$F_2 = \min \sum_{t=0}^{23} \sum_{k \in \mathbb{Q}} P_{\text{loss}}(k,t,a) \tag{5.2}$$

– Minimization of OLTC operational degradation:

$$F_3 = \min \sum_{t=0}^{23} |\Delta\text{tap}(t,a)| \tag{5.3}$$

Where $\mathbb{R} = \{3,7,10,16,21,24,25,30,32\}$ is the sets of RPV-connected buses; $P_{\text{RPV}}(m,t,a)$ represents the active power injected at node m and hour t under the action a from DRL, [kW]; $P_{\text{loss}}(k,t,a)$ is the active power loss sustained across branch k at hour t under the action a from DRL, [kW]; $\mathbb{Q}$ denotes the sets of grid branches; and $\Delta\text{tap}(t,a)$ quantifies the discrete mechanical step position of the OLTC under the action a from DRL.

5.2.2. Constraints

– Bus voltage boundaries: governed by formulation (3.4);

– Line current thermal limits: enforced via equation (3.3);
– Power flow equilibrium: sustained across the distribution network

$$P_{\text{gen},i} - P_{\text{load},i} + P_{\text{RPV},m} = V_i . \sum_{j \in \Omega_N} V_j \left(G_{ij} . \cos\theta_{ij} + B_{ij} . \sin\theta_{ij} \right) \quad (5.4)$$

$$Q_{\text{gen},i} - Q_{\text{load},i} \pm Q_{\text{inv},m} = V_i . \sum_{j \in \Omega_N} V_j \left(G_{ij} . \sin\theta_{ij} - B_{ij} . \cos\theta_{ij} \right) \quad (5.5)$$

– SI regulation capabilities: bound by active/reactive operational curves

$$P_{\text{inv}}^2(m,t,a) + Q_{\text{inv},m}^2(m,t,a) \le S_{\text{inv},m}^2(m,t,a) \quad (5.6)$$

– OLTC tap boundaries: restricted to discrete mechanical steps

$$-8 \le tap \le +8 \quad (5.7)$$

$$|\Delta tap(t,a)| \le 1 \quad (5.8)$$

5.2.3. Algorithm flowchart

The algorithm flowchart is shown in fig. 5.1.

5.2.4. Results and discussion

– DDQN training dynamics and policy evolution

Episodic reward fluctuates sharply over the initial 250 iterations due to agent experience, turning strictly non-negative from iteration 355 as RPV rewards outweigh penalties. Concurrently, $\mathcal{H}(\theta) = 2.34$ at iteration 5 and undergoes a 95% attenuation over the subsequent 250 iterations, verifying convergence. A critical voltage nadir of 0.7956 p.u. (20.4% drop) occurs at iteration 40 due to exploratory actions reducing tap_{OLTC} and suboptimally regulating SI during peak-load without RPV periods. Beyond iteration 1.250, $V_{\min}$ stabilizes around 0.95 p.u., with minor residual instability driven by extreme stochastic scenarios and a 1% random action probability. Ultimately, voltage violations contract to ~30% after 500 iterations and 16% after 1.000 iterations, validating robust operational constraint compliance.

At $t = 00{:}00$, $tap_{\text{OLTC}} = 0$ resets to 0; with RPV units inactive and $Q_{\text{inv}} = 0$, no voltage violations occur and control is omitted. At $t = 07{:}00$, load growth outpaces RPV ramp-up, increasing $tap_{\text{OLTC}} = +1$ under the average scenario and +2 under the cloudy scenario, while all RPV units inject Q_{inv} to support the $V_{\min}$. At midday, widespread voltage elevation prompts Q_{inv} inject along the main branch. At $t = 19{:}00$, peak demand coincides with the complete loss of RPV, driving tap_{OLTC} increments to +2 (average scenario), +3 (cloudy scenario), and +1 (remaining two scenarios), while all RPV units injects Q_{inv} to minimize network losses. The trained DRL policy establishes that tap_{OLTC} varies inversely with RPV output, and continuous diurnal Q_{inv} injection across the nine RPV nodes optimizes voltage regulation. Specifically, main-branch Q_{inv} injection at 01:00, 11:00, 14:00, and 16:00 fine-tunes voltage profiles at the three most sensitive buses (7, 16, and 30). Conversely, reactive power is absorbed along the main branch at 02:00 and

03:00 to mitigate voltage rises, whereas reactive power absorption from the external grid is completely avoided.

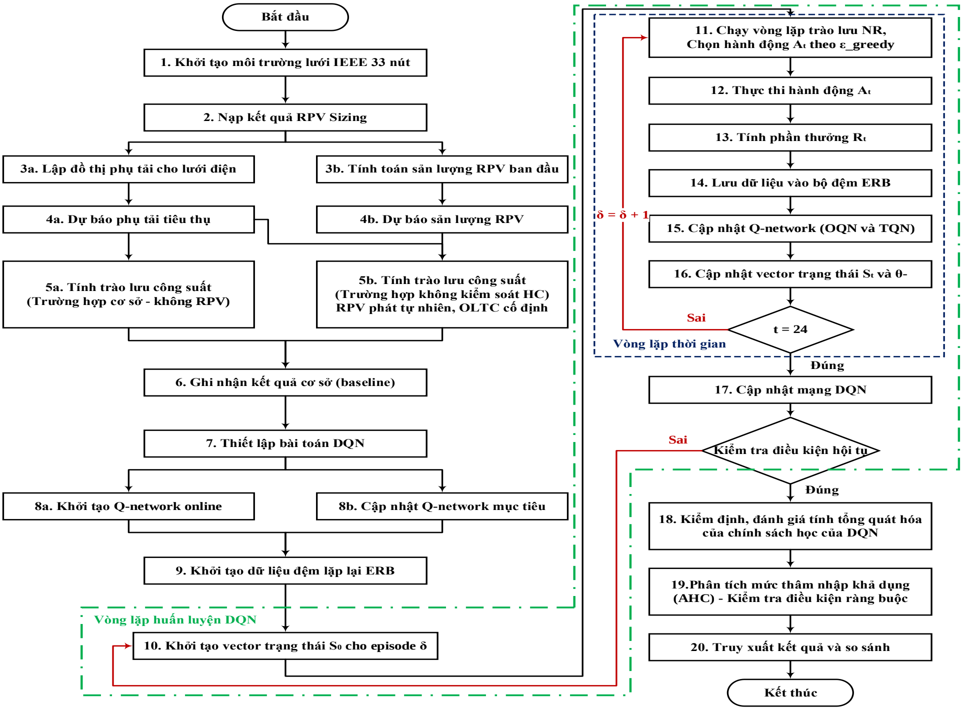

Fig 5.1. Procedural flowchart of the proposed DRL-driven multi-objective optimization framework.

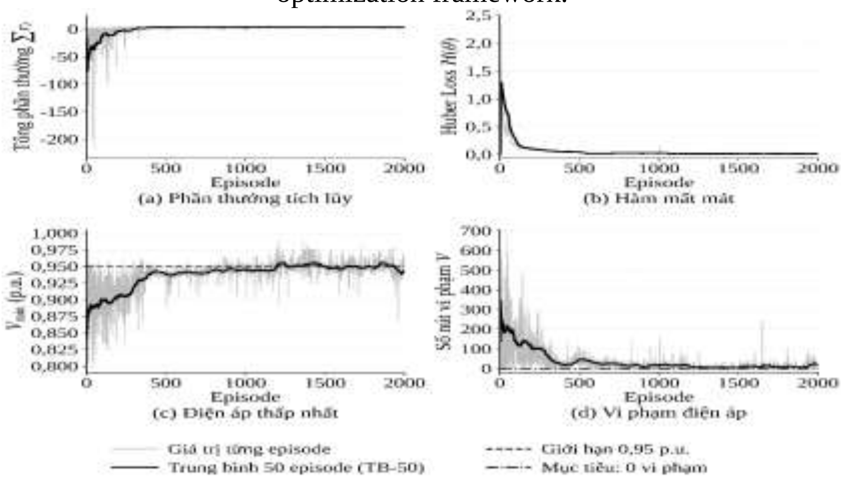

Fig 5.2. Convergence profiles of the proposed DDQN framework across the training horizon

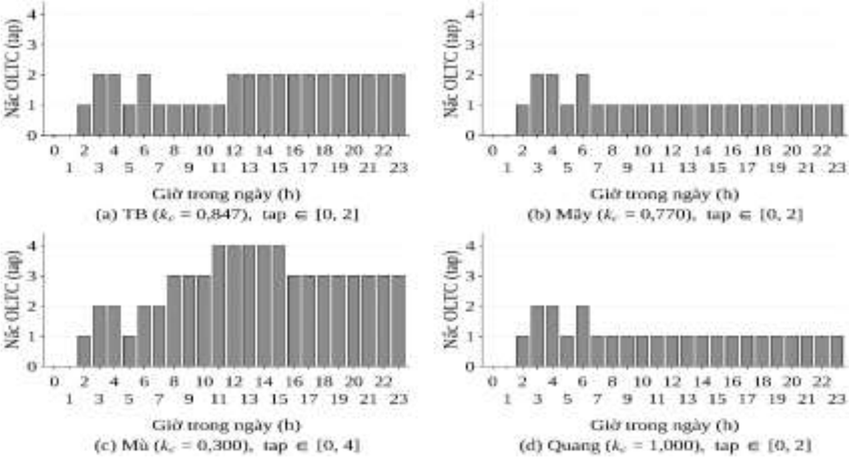

Fig 5.3. Adaptive trajectory of the learned OLTC tap-position control policy

– The sensitivity and voltage-margin analysis at the DRL operating point

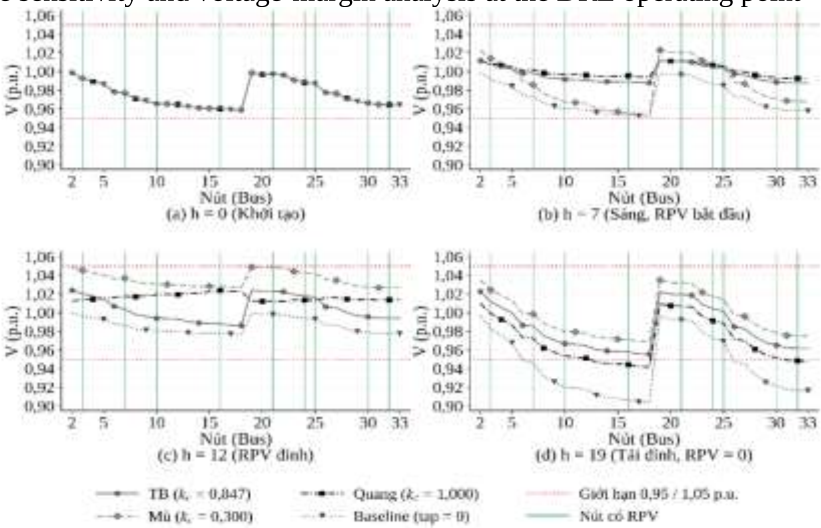

Fig 5.4. Grid voltage profiles across four critical operational hours

Midday analysis identifies node 16 at the most voltage-sensitive yet possessing the largest voltage margin, serving as the baseline for grid AHC determination and DDQN control guidance. This strategy prioritizes SI reactive power absorption at node 16 first, followed by other RPV units on the longest branch during high-irradiance periods. Conversely, node 21 exhibits the narrowest margin, requiring augmented reactive power injection to stabilize the 2-19-20-21 branch voltage under concurrent peak-RPV and high-load conditions. Although the aggregate decoupled capacity across the nine nodes totals ~23,077 kW at midday, this does not equal systemic AHC because it omits dynamic grid response capabilities.

– AHC assessment under voltage and line thermal constraints

Satisfying both voltage and thermal constraints determines the generation-increase factor ($k_{\text{cum.max}}$) for peak RPV AHC. Across clear sky, average, and cloudy scenarios, the system AHC converges uniformly to 9,320.9 kW. This boundary defines the absolute safety margin controllable by the DDQN framework before any violation occurs, yielding a 2.54-fold capacity enhancement over the standalone COOA optimization limit.

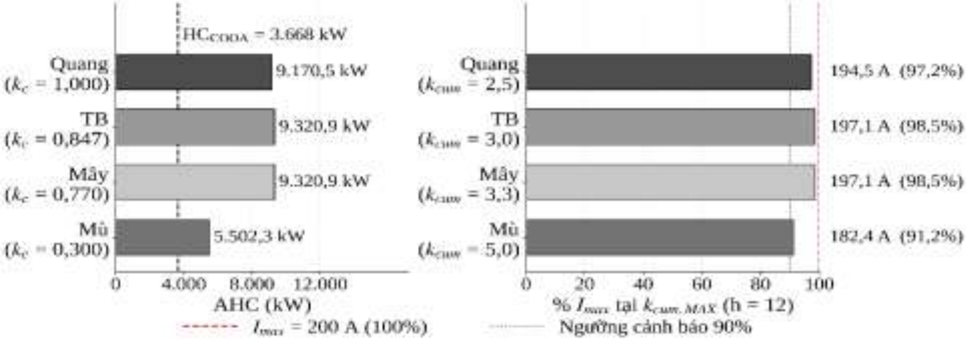

Fig 5.5. AHC evaluation results under voltage and line thermal constraints

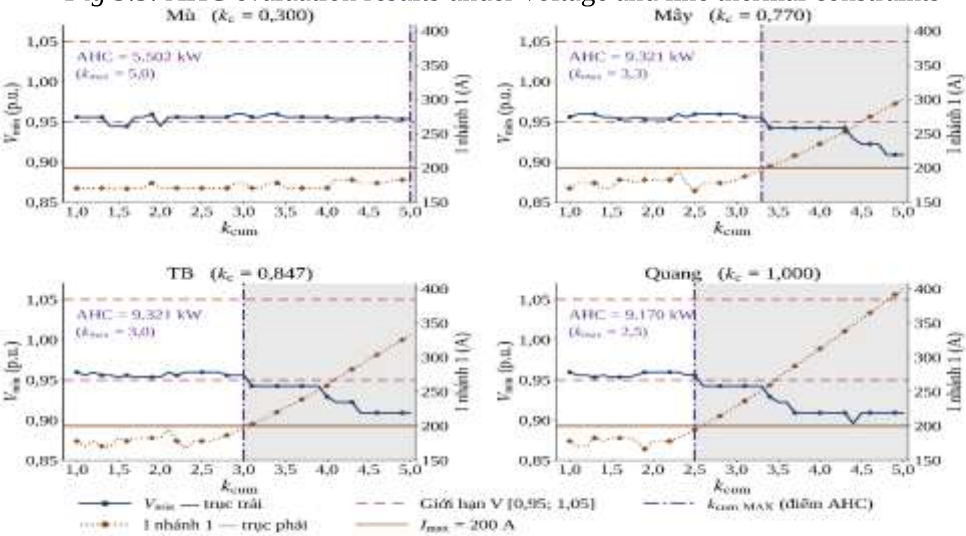

Fig 5.6. Network response under generation-increase factor parametric sweep

In the first chart, all trajectories surpass the 3,688.2 kW reference line, validating coordinated OLTC-SI efficacy, where each scenario-specific AHC marks the threshold preventing root-branch overloading. In the second chart, the 100% and 90% baselines define maximum thermal capacity and safety warning threshold, respectively. Keeping operating currents below 90% limits actual AHC to 204% - 231% of the baseline, yielding a 121% - 147% net penetration increment.

As shown in Fig. 5.6, each sub-chart maps 24-hour aggregate $V_{\min}$ [p.u.] and $I_{\max}$ [A] onto the left and right ordinates across specific k_c with violation markers denoting breaches during at least one hour. The cloudy scenario exhibits minimal variance, with minor, non-monotonic violations beyond $k_{\text{cum}} > 2$ due to DDQN policy sensitivity rather than network physics, risking no reverse power overflow. However, it maintains $V_{\min} > 0.95$ [p.u.] before abruptly collapsing past $k_{\text{cum}} = 3$. The average scenario mirrors this trend but experiences voltage instability earlier at $k_{\text{cum}} = 2{,}6$, with its operating current linearly breaching thresholds at $k_{\text{cum}} = 3{,}1$. Concurrently, the clear-sky scenario triggers simultaneous dual-constraint violations at $k_{\text{cum}} = 2{,}6$, where premature DDQN reactive power absorption to suppress overvoltage causes early SI saturation. These metrics verify that: (i) V-I bounds experience simultaneous dual violations without hierarchical priority; and (ii) $V_{\min}$ degrades rapidly post-saturation, demonstrating that SI absorption saturation invalidates DDQN controllability and renders the OLTC ineffective.

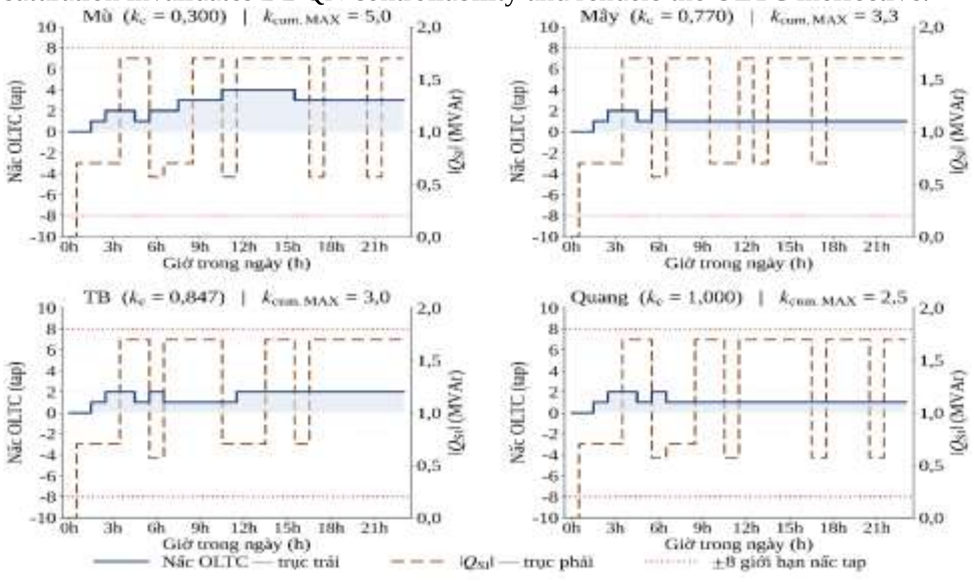

Fig 5.7. Coordinated OLTC and SI scheduling profiles

Fig. 5.7 maps six chronological stages across four scenarios: (1) 01:00 – 03:00: To counteract midnight undervoltages, all scenarios increment the tap from 0 to +1 (at 02:00) then +2 (at 03:00), while SIs inject Q_{inv} at nodes 7, 16, and 30; (ii) 03:00 – 07:00: The tap stays at +2, SIs inject Q_{inv} at 9 RPV buses during low-load periods, switching to localized absorption by 06:00 as initial RPV generation prompts overvoltage mitigation; (iii) 07:00 – 10:00: As RPV penetration escalates from 28.8% to 69.5%, the tap is held at +2, and SIs execute identical, coordinated

Q_{inv} absorption along the main branch; (iv) 10:00 – 13:00: Scenarios diverge; the overcast scenario avoids reverse power flow, lowering its tap to +1 at 11:00 (sustained until 13:00) with zero SI activation. Conversely, the other three scenarios undergo reverse power flow, forcing a three-step consecutive tap reduction to -1 while all nine SIs maximize absorption to suppress V-I violations; (v) 13:00 – 17:00: Coinciding with declining P_{RPV}, tap recover to +1 by 17:00, and SIs modulate from absorption to idle; and (vi) 17:00 – 00:00: With $P_{\text{RPV}} = 0$, the tap advances to +3, and all nine SIs inject Q_{inv} to stabilize the net-load voltage profile.

These findings verify that: (i) the DDQN framework establishes a robust control policy with an operational safety margin; (ii) The OLTC physical dwell-time constraint acts as the binding hard constraint governing system AHC; (iii) SI $Q_{\text{inv.max}}$ absorption during stage 4 introduces localized overloading risks along the source-proximal branch; and (iv) The OLTC mechanism is immune to saturation. Furthermore, embedding thermal constraints directly into the reward formulation would expand the permissible RPV penetration threshold.

5.2.5. Comparative evaluation

Methodologically, DDQN is benchmarked against [13], [14], [15], [16], [17], and [18]: (i) it executes discrete actions matching OLTC mechanics, utilizing only 24,213 parameters to minimize computation – far fewer than [13] – [18]; (ii) six models share identical IEEE 33-bus parameters and constraints; (iii) DDQN integrates 50 RPV/load scenarios for coverage; (iv) DDQN uniquely employs four solar-irradiance scenarios for AHC evaluation; and (v) it additionally enforces line thermal limits. All seven approaches eliminate voltage violations while minimizing losses and operating costs.

For AHC performance, DDQN is compared with methodologically similar benchmarks [19], [20] and [21], where literature-wide penetration gains range from 60% to 200%. Specifically, [19] achieves 229% AHC via maximal control devices, yet permits minor voltage violations and neglects thermal constraints. Omitting grit-wide regulation due to dispersed loads and long lines in a rural network, [20] applies PSO for localized RPV Volt-VAr setpoints, yielding 174.8% static penetration and 44.3% AHC improvement. By minimizing customer costs, [21] establishes a 113% maximum penetration and 49.2% AHC enhancement. In comparison, the proposed DDQN attains a 121% to 147% penetration increment over the COOA baseline.

CHAPTER 6. CONCLUSION AND FUTURE WORKS

6.1. Conclusion

This dissertation analyzes high-penetration RPV impacts on MV grid current, voltage, and losses, proposing two penetration determination models and one selective power curtailment scheme to ensure secure, economic operation across four addressed problems.

Problem 1 investigates rapid PV penetration into MV grids lacking utility operational experience. Grid deployment of seven RPV sources (~650 kWp) demonstrates that moderate penetration optimizes power-loss profiles; however, penetration exceeding 85% violates loss thresholds, and a 135% level overloads all feeder transformers.

Problem 2 establishes an optimal RPV curtailment methodology to mitigate irrational integration planning. Because curtailed energy depends on busbar source voltage, extreme-condition curtailment must be evaluated grid-wide. Under baseline voltage and favorable sunny conditions, a 9.28 MWp capacity permits up to 190.4% load penetration without violations. Conversely, elevated source voltages trigger exponential V-I violations, driving daily curtailment ratios to 21.08% - 48.69%, optimized effectively via the BA.

Problem 3 optimizes RPV allocation sites, installed capacities, and power factors using COOA integrated with FBS to minimize total active power loss. Across both benchmark networks, COOA outperforms alternative MH. Under a fixed unity power factor, RPV penetration strictly matches grid demand; relaxing power factor, site, and unit count constraints yields a penetration range of 65% - 115% of peak load. Fixed-parameter configurations achieve 65.50% and 69.14% loss reductions for the respective networks, whereas flexible self-optimization by COOA drives grid loss reduction beyond 99%.

Problem 4 proposes a DDQN framework combining DRL self-adaptation and ANN data-processing for grid control. Managing three optimization objectives, the model leverages OLTC and SI for adaptive Volt-VAr regulation. Post-500 training iterations, DDQN achieves autonomous grid control, with line thermal and voltage boundaries dictating system AHC. Under scaling RPV penetration, AHC fluctuates non-monotonically with irradiance, capping at 150% (cloudy), 254.1% (overcast/ average), and 250% (clear-sky) of load demand. Notably, incorporating peak ambient and RPV operating temperatures degrades simulated AHC by up to 30%.

6.2. Future works

Despite achieved milestones, future research will address the following independent or concurrent vectors: (i) extending HC_{RPV} và AHC frameworks to low-voltage networks; (ii) transitioning from forecasted models to historical and real-time operational data; (iii) integrating energy storage and advanced voltage regulators under diversified loads; (iv) analyzing meshed MV grid topologies; (v) incorporating multi-objective optimization under expanded operational constraints; and (vi) developing hybrid algorithms and pursuing experimental validation on an active Vietnamese feeder.

REFERENCES

[1] M. Karimi, H. Mokhlis, K. Naidu, S. Uddin and A. H. A. Bakar, "Photovoltaic penetration issues and impacts in distribution network - A review," *Renewable and Sustainable Energy Reviews,* vol. 53, pp. 594-605, 2016.

[2] S. M. Ismael, S. H. E. A. Aleem, A. Y. Abdelaziz and A. F. Zobaa, "State-of-the-art of hosting capacity in modern power systems with distributed generation," *Renewable Energy,* vol. 130, pp. 1002-1020, 2019.

[3] Vietnam, "Quyết định số 768/QĐ-TTg của Thủ tướng Chính phủ: Phê duyệt Điều chỉnh Quy hoạch phát triển điện lực quốc gia thời kỳ 2021 - 2030, tầm nhìn đến năm 2050," Chính phủ nước Cộng hòa Xã hội Chủ nghĩa Việt Nam, Hà Nội, 2025.

[4] S. Remha, C. Saliha and S. Arif, "A Novel Multi-Objective Bat Algorithm for Optimal Placement and Sizing of Distributed Generation in Radial Distributed Systems," *Advances in Electrical and Electronic Engineering,* vol. 15, no. 5, pp. 736-746, 2018.

[5] I. Naruei and F. Keynia, "A new optimization method based on COOT bird natural life model," *Expert Systems with Applications,* vol. 183, p. 115352, 2021.

[6] M. E. Baran and F. F. Wu, "Network reconfiguration in distribution systems for loss reduction and load balancing," *IEEE Transactions on Power Delivery,* vol. 4, no. 2, pp. 1401-1408, 1989.

[7] T. N. Thuan, T. N. Thang and V. V. Cuong, "Reconfiguration of Distribution Network Considering Photovoltaic System Placement Based on Metaheuristic Algorithms," in *Advances in Artificial Intelligence for Renewable Energy Systems and Energy Autonomy*, Switzerland, Springer Nature Link Switzerland, 2023, pp. 135-156.

[8] M. Massaoudi, H. Abu-Rub and A. Ghrayeb, "Navigating the Landscape of Deep Reinforcement Learning for Power System Stability Control: A Review," *IEEE Access,* vol. 11, pp. 134298-134317, 2023.

[9] Y. Li, J. Wu and Y. Pan, "Deep reinforcement learning for online scheduling of photovoltaic systems with battery energy storage systems," *Intelligent and Converged Networks,* vol. 5, no. 1, pp. 28-41, 2024.

[10] Y. Cui, Y. Xu, Y. Li, Y. Wang and X. Zou, "Deep Reinforcement Learning Based Optimal Energy Management of Multi-energy Microgrids with Uncertainties," *CSEE Journal of Power and Energy Systems,* vol. 12, no. 2, pp. 1002-1014, 2026.

[11] L. Yan and C. Cheng, "Voltage Control for Distribution Networks Based on Large Language Model-Assisted Deep Reinforcement Learning," *IEEE Power & Energy Society Section,* vol. 13, pp. 76072-76084, 2025.

[12] M. Zhang, G. Guo and T. X. Q. Zhao, "DNN Assisted Projection Based Deep Reinforcement Learning for Safe Control of Distribution Grids," *IEEE Transactions on Power Systems,* vol. 39, no. 4, pp. 5687-5698, 2024.

[13] D. Cao, W. Hu, J. Zhao, Q. Huang, Z. Chen and F. Blaabjerg, "A Multi-Agent Deep Reinforcement Learning Based Voltage Regulation Using Coordinated PV Inverters," *IEEE Transactions on Power Electronics,* vol. 35, no. 5, pp. 4120-4123, 2020.

[14] M. Ma, W. Du, L. Wang, C. Ding and S. Liu, "Research on the multi-timescale optimal voltage control method for distribution network based on a DQN-DDPG algorithm," *Frontiers in Energy Research*, 2022.

[15] R. Hossain, M. Gautam, J. Thapa, H. Livani and M. Benidris, "Deep reinforcement learning assisted co-optimization of Volt-VAR grid service in distribution networks," *Sustainable Energy, Grids and Networks*, vol. 35, p. 101086, 2023.

[16] J. Suchithra, D. A. Robinson and A. Rajabi, "A Model-Free Deep Reinforcement Learning-Based Approach for Assessment of Real-Time PV Hosting Capacity," *Energies*, vol. 17, p. 2075, 2024.

[17] D. Hua, F. Peng, S. Liu, Q. Lin, J. Fan and Q. Li, "Coordinated Volt/VAR Control in Distribution Networks Considering Demand Response via Safe Deep Reinforcement Learning," *Energies*, vol. 18, no. 2, p. 333, 2025.

[18] K. Xiong, C. Ye, B. Liu and X. Suo, "Multi-agent deep reinforcement learning-enabled voltage regulation approach for partitioned active distribution network using heterogeneous PV inverters," *Energy Conversion and Economics*, vol. 6, no. 6, pp. 359-370, 2025.

[19] A. Ali, K. Mahmoud and M. Lehtonen, "Maximizing Hosting Capacity of Uncertain Photovoltaics by Coordinated Management of OLTC, VAr Sources and Stochastic EVs," *International Journal of Electrical Power & Energy Systems*, vol. 127, p. 106627, 2021.

[20] B. Jaramillo-Leon, S. Zambrano-Asanza, J. F. Franco and J. B. Leite, "Simulation-based optimization framework to increase distribution system photovoltaic hosting capacity through optimal settings of smart inverter Volt-VAr control function," *Electric Power Systems Research*, vol. 215, no. A, p. 108971, 2023.

[21] Z. M. Zenhom, S. H. E. A. Aleem, E. A. Zahab and T. A. Boghdady, "Simultaneous distributed generation and electric vehicles hosting capacity enhancement through a synergetic hierarchical bi-level optimization approach based on demand response and Volt/VAR control," Scientific Report, Ai Cập, 2025.